Luminescent properties of rare-earth-doped $CaWO_4$ phosphor films prepared by the Pechini sol–gel process

2003 J. Phys.: Condens. Matter 15 5157

(http://iopscience.iop.org/0953-8984/15/29/327)

INSTITUTE OF PHYSICS PUBLISHING JOURNAL OF PHYSICS: CONDENSED MATTER

J. Phys.: Condens. Matter **15** (2003) 5157–5169 PII: S0953-8984(03)61729-7

Luminescent properties of rare-earth-doped $CaWO_4$ phosphor films prepared by the Pechini sol–gel process

M L Pang, J Lin[1], S B Wang, M Yu, Y H Zhou and X M Han

Key Laboratory of Rare Earth Chemistry and Physics, Changchun Institute of Applied Chemistry, Chinese Academy of Sciences, Changchun 130022, People's Republic of China

E-mail: jlin@ns.ciac.jl.cn

Received 2 April 2003, in final form 20 May 2003
Published 11 July 2003
Online at stacks.iop.org/JPhysCM/15/5157

Abstract

$CaWO_4$ phosphor films doped with rare-earth ions (Eu^{3+}, Dy^{3+}, Sm^{3+}, Er^{3+}) were prepared by the Pechini sol–gel process. X-ray diffraction (XRD), Fourier transform infrared spectroscopy, thermogravimetric and differential thermal analysis, atomic force microscopy, and photoluminescence spectra, as well as lifetimes, were used to characterize the resulting powders and films. The results of the XRD analysis indicated that the films began to crystallize at 400 °C and that the crystallinity increased with elevation of the annealing temperature. The doped rare-earth ions showed their characteristic emissions in crystalline $CaWO_4$ phosphor films due to energy transfer from WO_4^{2-} groups to them. Both the lifetimes and PL intensities of the doped rare-earth ions increased with increasing annealing temperature, from 500 to 900 °C, and the optimum concentrations for Eu^{3+}, Dy^{3+}, Sm^{3+}, Er^{3+} were determined as 30, 1.5, 1.5, 0.5 at.% of Ca^{2+} in $CaWO_4$ films annealed at 900 °C, respectively.

1. Introduction

Because of their attractive luminescence and structural properties [1], tungstates have been intensively studied and applied in many fields such as those of lasers, fluorescent lamps, and scintillators during the past few decades. As a representative example, calcium tungstate ($CaWO_4$) with the scheelite structure, which is built from Ca^{2+} ions and WO_4^{2-} groups with the coordination numbers of eight for Ca^{2+} and four for W^{6+} [2–4], is considered to be a highly functional material due to its intriguing luminescent properties [5–7]. It mainly shows an efficient blue emission excited by short-wavelength ultraviolet radiation, x-rays, cathode rays, etc.

It is well known that luminescent films play an important role in high-resolution devices such as cathode-ray tubes (CRTs), electroluminescent devices (ELDs), plasma display panels

[1] Author to whom any correspondence should be addressed.

(PDPs), and field emission displays (FEDs) [8]. Displays with thin-film phosphors have higher contrast and resolution, superior thermal conductivity, as well as a high degree of uniformity and better adhesion [9]. Various preparation methods have been employed to prepare $CaWO_4$ luminescent films, such as spray pyrolysis [10], sputtering deposition [11], electron beam evaporation [12], and electrochemical deposition [4, 13, 14]. Generally, these techniques need expensive and complicated equipment set-ups. Therefore, a simple and economical method for making high-quality luminescent films is desirable. The solution-based sol–gel method is one of the most important techniques for the synthesis of various functional coating films, because it possesses a number of advantages over conventional film formation techniques, such as low-temperature processing, easy coating of large surfaces, and possible formation of porous films and homogeneous multicomponent oxide films [15]. In fact, some efforts have been made to develop various kinds of luminescent film via a sol–gel method in the past decade. Representative examples are $Y_3Al_5O_{12}$:Tb [8] and Y_2SiO_5:Tb [9] films for cathodoluminescence, $Y_3Al_5O_{12}$:Eu [16] films for FEDs, Y_2O_3:Eu [17] and Zn_2SiO_4:Mn [18] films for photoluminescence. In most of the above cases, the sol–gel precursors used are metal alkoxides and/or organometallic compounds, which suffer from the disadvantages of high cost, toxicity, and difficulty in controlling the experimental processes. An alternative approach to forming thin films is a Pechini-type sol–gel process, which mainly employs inorganic salts as precursors, citric acid as the chelate ligand, and polyethylene glycol (PEG) as the cross-linking agent [19].

To our knowledge, so far no paper has been published on the preparation of rare-earth-ion-doped $CaWO_4$ films by the Pechini sol–gel process. In view of this and the high cost and toxicity of the alkoxide precursors used in the conventional sol–gel process, we carried out a Pechini sol–gel synthesis of $CaWO_4$ thin-film phosphors doped with rare-earth ions (Eu^{3+}, Dy^{3+}, Sm^{3+}, Er^{3+}), which we report on in this paper, together with their photoluminescence properties.

2. Experimental section

2.1. Preparation of the films

The thin-film phosphor samples of $Ca_{1-x}RE_xWO_4$ ($0 \leqslant x \leqslant 0.5$; RE = Eu^{3+}, Dy^{3+}, Sm^{3+}, Er^{3+}) were prepared by a Pechini sol–gel and dip-coating method [20]. Stoichiometric amounts of $CaCO_3$ (analytical reagent, AR), Eu_2O_3 (99.99%), Dy_2O_3 (99.99%), Sm_2O_3 (99.99%), and Er_2O_3 (99.99%) were dissolved in dilute HNO_3 (AR) while vigorously stirring, and the pH value of the solution was kept between two and three. Then a stoichiometric amount of ammonium tungstate $(NH_4)_{10}W_{12}O_{41}\cdot 5H_2O$ (Fluka) and a suitable amount of water–ethanol solution containing citric acid (AR) as the chelating agent for the metal ions were added to the solution. The molar ratio of metal ions to citric acid was 1:2. A certain amount of polyethylene glycol (PEG; molecular weight: 10 000, AR) was added as the cross-linking agent. Highly transparent sols were obtained after stirring for a few hours, and these were subsequently used for film deposition.

Silica glasses were used as the substrates. These were precleaned in a 5% KOH solution for 15 min; this procedure was followed by a 5 min dipping in 1.0 M HCl to neutralize the alkali attack on the glass surface, and then soaking in pure water for 20 min. Finally they were thoroughly ultrasonicated in ethanol for 20 min. The thoroughly cleaned silica glass substrates were dipped into the sols and withdrawn at a speed of 0.5 cm s^{-1}. The as-formed transparent films were dried at 120 °C immediately to drive off the remaining solvent. Then the films were annealed to high temperatures (300–900 °C) with a heating rate of 60 °C h^{-1} and held at each

temperature for 2 h. In some cases, powder samples were used for the characterization (FT-IR, TG-DTA). These powders were produced by evaporating the above sols to dry gels in a water bath at 70 °C, and drying at 100 °C; then the same annealing procedures as for the films were utilized.

2.2. Characterization

The x-ray powder diffraction (XRD) of the film samples was examined using a Rigaku-Dmax 2500 diffractometer using Cu Kα radiation ($\lambda = 0.154\,056$ nm). FT-IR spectra were measured with Perkin-Elmer 580B infrared spectrophotometer with the KBr pellet technique. A TA Instruments (USA) thermal analyser was used to record TG-DTA curves for the gel powders in the open atmosphere. The morphology of the films was measured using an atomic force microscope (AFM, Seiko) with a tapping mode. The thickness of the films was obtained using an AUEL-III automatic laser ellipsometer. The excitation and emission spectra were obtained using a F-4500 spectrofluorimeter equipped with a 150 W xenon lamp as the excitation source. Luminescence lifetimes were measured with a SPEX 1934D phosphorimeter using a 7 W pulse xenon lamp as the excitation source with the pulse width of 3 μs. All the measurements were performed at room temperature.

3. Results and discussion

3.1. Formation process and morphology of the phosphor films

Since the results of the XRD, FT-IR, TG-DTA, AFM studies are independent of the doped rare-earth ions and their concentrations in $CaWO_4$, we confine ourselves to the $Ca_{0.95}Eu_{0.05}WO_4$ samples to elucidate the formation process and morphology of the phosphor films.

XRD. Figure 1 shows the XRD profiles of the $Ca_{0.95}Eu_{0.05}WO_4$ films annealed from 300–900 °C (a) and JCPDS Card 41-1431 data for $CaWO_4$ (b) as a reference. For the films annealed at 300 °C, no diffraction peak is observed except for a broad band at $2\theta \approx 22°$, which is ascribed to the silica glass substrate. This indicates that the film remains amorphous at or below this annealing temperature. For the sample fired at 400 °C, an intense diffraction peak at $2\theta \approx 28.5°$ and several weak diffraction peaks at $2\theta \approx 18.6°$, 31.4°, 34.2°, 47.1°, 54.3°, 57.9°, and 76.2° are present in the XRD pattern, which are assigned to the (112), (101), (004), (200), (204), (116), (312), and (316) reflections of tetragonal $CaWO_4$ respectively, suggesting the onset of crystallization at this stage. Further increase of the annealing temperature from 500 to 900 °C leads these peaks to become sharper and stronger due to the increase in crystallinity. All the diffraction peaks are in complete agreement with those of JCPDS Card 41-1431 for $CaWO_4$ (figure 1(b)).

FT-IR. The FT-IR spectra of the $Ca_{0.95}Eu_{0.05}WO_4$ gel powders annealed from 100–900 °C are shown in figure 2. For the sample dried at 100 °C, the FT-IR spectrum shows several broad absorption bands of the –OH group (3432 cm^{-1}), the $-CH_2$ group (2918 cm^{-1}), the NO_3^- group (1735, 1627 cm^{-1}), the carbonate COO^- group (1399, 1353 cm^{-1}), and the $W_{12}O_{41}^{10-}$ group (950, 890, 793, 596 cm^{-1}), all of which arise from the starting materials such as citric acid, PEG, $Eu(NO_3)_3$, $Ca(NO_3)_2$, and $(NH_4)_{10}W_{12}O_{41}{\cdot}5H_2O$, as observed previously [20–22]. The absorption intensities of these bands decreased with increasing sintering temperature due to the pyrolysis of the organic species. For the sample annealed at 300 °C, the FT-IR spectrum still shows several broad absorption bands at 3402, 2964, 1712, 1573, 1408, 1315 cm^{-1}, indicating

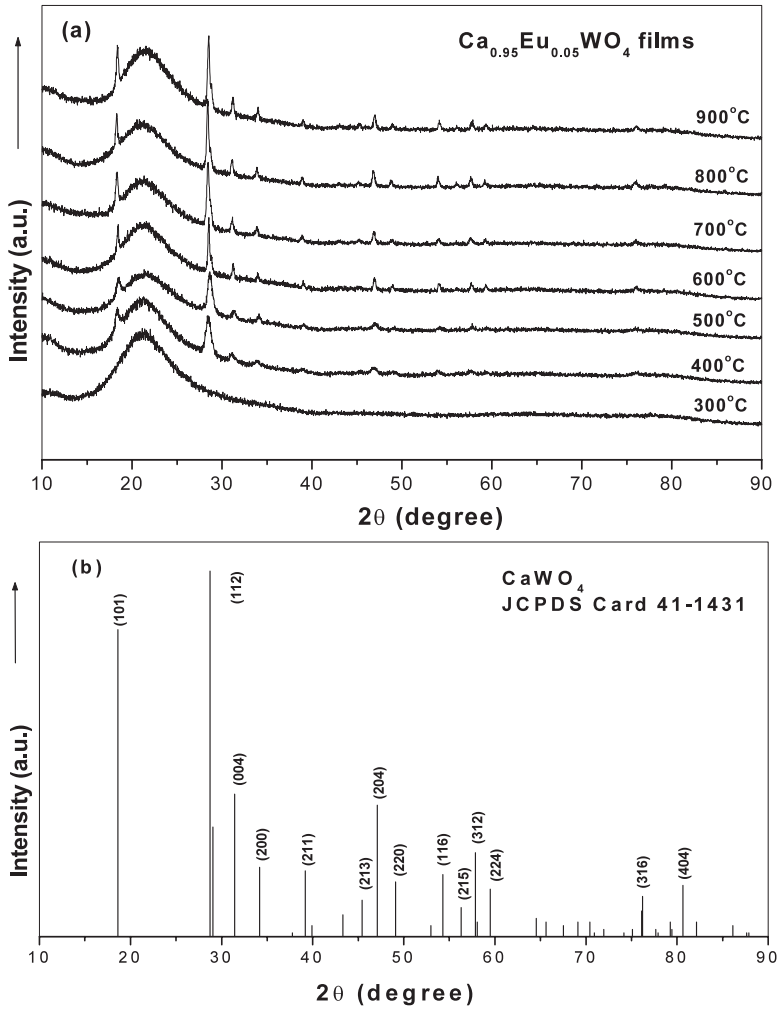

Figure 1. X-ray diffraction patterns for $Ca_{0.95}Eu_{0.05}WO_4$ films annealed at different temperatures (a) and JCPDS Card 41-1431 data for $CaWO_4$ (b).

that the organic species have not decomposed completely at this stage. After heating to 400 °C, although the organic impurities can still be observed in the FT-IR spectra of the samples, a very strong absorption peak at 807 cm^{-1} has appeared, which relates to the W–O stretching vibration mode (ν_3) for the crystalline $CaWO_4$ phase [23]. This suggests that crystalline $CaWO_4$ has formed at this temperature (400 °C), agreeing basically with the results of XRD analysis. After further heat treatment from 500 to 900 °C, the absorption of organic impurities gradually disappeared, and the W–O bond becomes stronger due to the improvement in crystallinity with increase in the annealing temperature. At 900 °C, there are also two weak and broad peaks at 3400 and 1650 cm^{-1}, which may be due to the H_2O absorbed in the course of the measurement.

TG-DTA. The precursor solution was evaporated to yield powder, which was analysed by TG-DTA in the open atmosphere. Figure 3 shows the TG-DTA curves for the $Ca_{0.95}Eu_{0.05}WO_4$ gel powder obtained at a heating rate of 10 °C min^{-1}. The TG curve shows three stages of

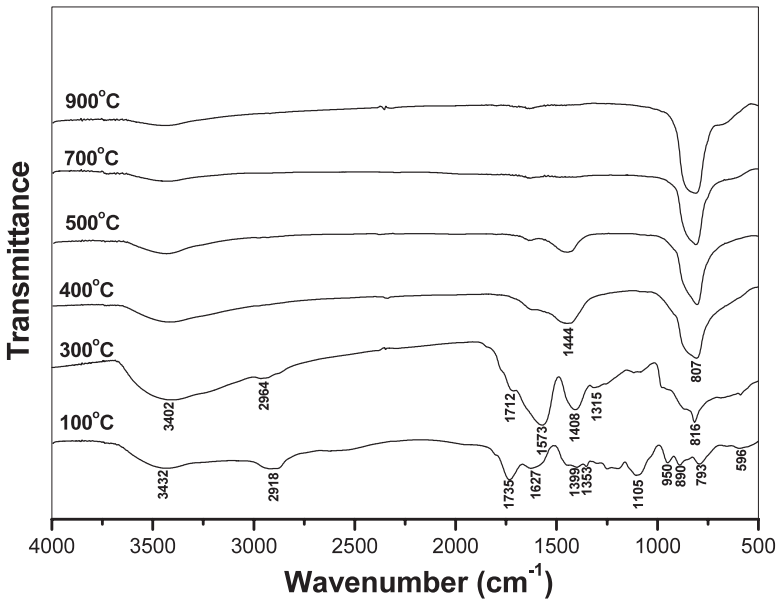

Figure 2. FT-IR spectra of $Ca_{0.95}Eu_{0.05}WO_4$ precursor powders annealed at different temperatures.

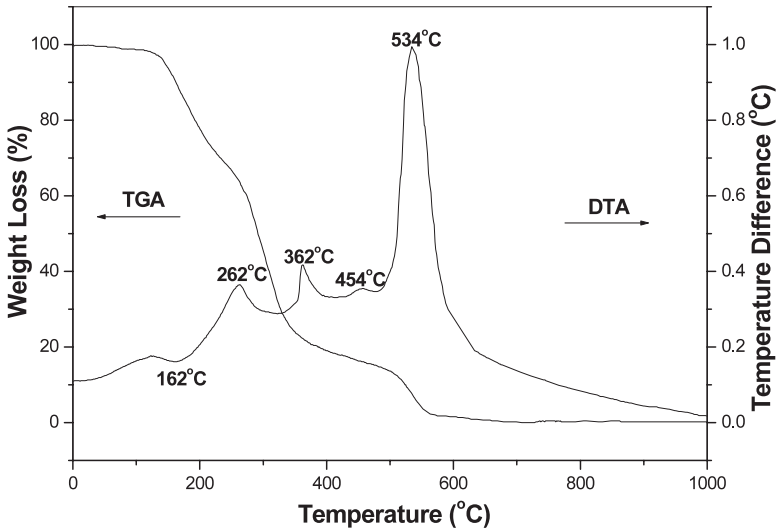

Figure 3. TG-DTA curves for $Ca_{0.95}Eu_{0.05}WO_4$ gel powder.

weight loss. The first weight loss (30%) step is observed between 20 and 220 °C, accompanied by an endothermic peak at 162 °C in the DT curve due to the evaporation of water and organic solvents [20]. The second weight loss (45%) is from 220 to 340 °C, accompanied by a strong exothermic peak at 262 °C in the DT curve due to the burn-out of excess solvents. The third weight loss step (25%) is noticed between 340 and 560 °C, accompanied by three exothermic peaks at 362, 454, and 534 °C in the DT curve. The two strong exothermic peaks at 362 °C and 534 °C in the DT curve are caused by the further combustion of the organic groups in PEG,

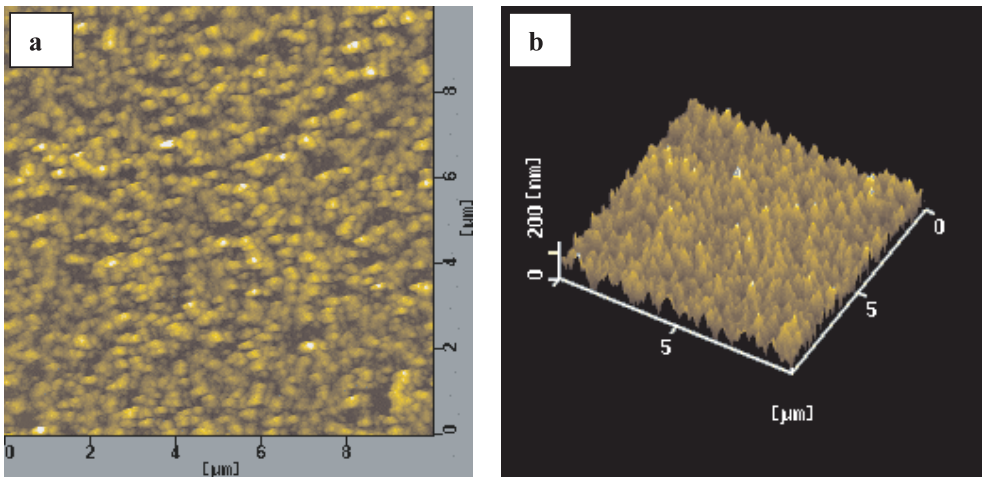

Figure 4. AFM micrographs of crystalline $Ca_{0.95}Eu_{0.05}WO_4$ film annealed at 900 °C: (a) planar image; (b) stereo image.

(This figure is in colour only in the electronic version)

citric acid, and the polyester (formed by the reaction between PEG and citric acid), as well as the citrates [20], while the weak exothermic peak at 454 °C in the DTA curve is probably due to the crystallization of the $CaWO_4$ phase, basically agreeing with the results of the XRD and FT-IR analysis.

Morphology of the films. A single layer of the $Ca_{0.95}Eu_{0.05}WO_4$ film has a thickness of about 200 nm, measured using an AUEL-III automatic laser ellipsometer. The morphology of the crystalline $Ca_{0.95}Eu_{0.05}WO_4$ film sample was inspected using an atomic force microscope (AFM). Figure 4 shows the AFM images of the transparent $Ca_{0.95}Eu_{0.05}WO_4$ film annealed at 900 °C. It is known from planar images that the film is uniform and crack-free, and mainly consists of closely packed fine particles with an average grain size of 130 nm (see the planar image in figure 4(a)), and the surface is well crystallized and very smooth with a root mean square (RMS) roughness of 4–5 nm (see the stereo image in figure 4(b)).

3.2. Photoluminescence properties

Spectral properties of $CaWO_4$ films doped with rare-earth ions (Eu^{3+}, Dy^{3+}, Sm^{3+}, Er^{3+}). It is well known that $CaWO_4$ may show different emissions in the blue, green, blue–green, and red regions depending on the different excitation wavelengths or energy [6, 7, 24, 25]. Most of the studies and applications have been focused on the blue emission [24, 25]. In this work, we first prepared an undoped $CaWO_4$ film to study its intrinsic luminescent properties, and then doped four kinds of rare-earth ion (Eu^{3+}, Dy^{3+}, Sm^{3+}, Er^{3+}) into the $CaWO_4$ film hosts to find out the optimal conditions for strong photoluminescence.

Figure 5 shows the excitation (a) and emission (b) spectra of the undoped $CaWO_4$ film (annealed at 900 °C) in the UV/visible region. Under short-wavelength UV excitation, the $CaWO_4$ film exhibits a strong blue emission with a maximum at 415 nm, which can be seen clearly from the emission spectrum (figure 5(b)). It is well known that with the excitation from O_{2p} to $W_{t_{2g}}$, the WO_4^{2-} groups absorb ultraviolet irradiation in $CaWO_4$. In the excited

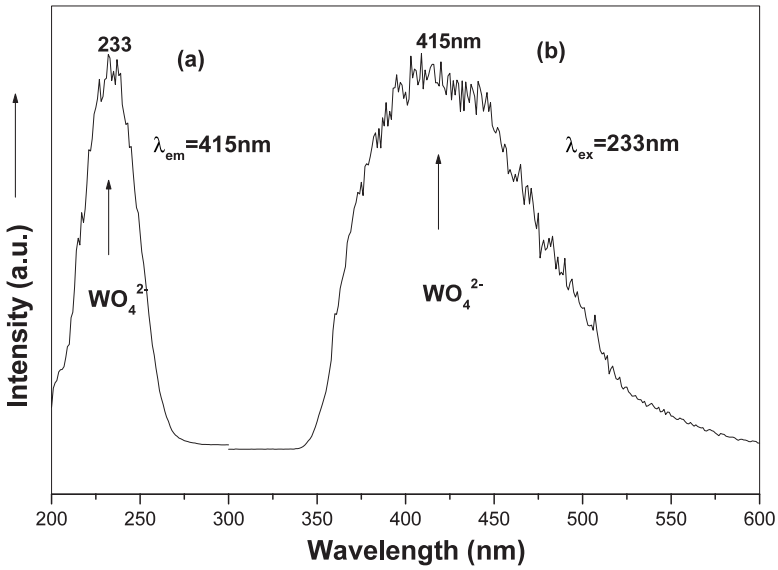

Figure 5. Excitation (a) and emission (b) spectra of $CaWO_4$ films annealed at 900 °C.

state of the WO_4^{2-} groups, the hole (on the oxygen) and the electron (on the tungsten) remain together as an exciton because of their strong interactions [5]. This optical band-edge excitation yields a strong blue emission [14]. The excitation spectrum was obtained by monitoring the emission of WO_4^{2-} at 415 nm (figure 5(a)). It can be seen that the excitation spectrum consists of an intense broad band with a maximum at 233 nm. Obviously, this band is ascribed to a charge transfer from the oxygen ligand to the central tungsten atom inside the WO_4^{2-} ion. It is generally considered that the excitation and emission spectra obtained are mainly due to the charge-transfer transitions within the WO_4^{2-} complex [26]. In other words, the intense broad band appearing in the excitation spectrum arises from the $CaWO_4$ host lattice.

Figure 6 shows the excitation (a) and emission (b) spectra for $Ca_{0.7}Eu_{0.3}WO_4$ film annealed at 900 °C in the UV/visible spectral range. The excitation spectrum was obtained by monitoring the emission of the Eu^{3+} $^5D_0$–$^7F_2$ transition at 614 nm. It can be seen clearly that the excitation spectrum mainly consists of a broad intense band with a maximum at 243 nm and some weak lines in the longer-wavelength region. Considering the excitation spectrum for the undoped $CaWO_4$ film in figure 5, the broad excitation band for $Ca_{0.7}Eu_{0.3}WO_4$ film can be attributed to the $CaWO_4$ host lattice, i.e., the absorption of WO_4^{2-} groups, and the other weak lines in the longer-wavelength region are due to the f–f transitions within the Eu^{3+} $4f^6$ electron configuration. The presence of the strong absorption band of WO_4^{2-} groups in the excitation spectrum of Eu^{3+} indicates that there is an energy transfer from WO_4^{2-} groups to Eu^{3+} ions in $Ca_{0.7}Eu_{0.3}WO_4$ film. Upon excitation into the WO_4^{2-} absorption band at 243 nm, we can not only observe the weak emission from the WO_4^{2-} groups from 350 to 550 nm, but also the strong emissions corresponding ^5D_J–$^7F_{J'}$ ($J = 0, 1, 2$; $J' = 0, 1, 2, 3, 4$, not in all cases) transitions of Eu^{3+}. The locations of the emission lines of Eu^{3+} and their assignments are indicated in the figure. Compared with the emissions of Eu^{3+}, the intrinsic blue emission from WO_4^{2-} is very weak, suggesting that an efficient energy transfer from WO_4^{2-} to Eu^{3+} has occurred. The emission spectrum of Eu^{3+} is dominated by the hypersensitive red emission $^5D_0$–$^7F_2$ transition of Eu^{3+} at 614 nm (as indicated in figure 6(b)). This indicates that the Eu^{3+} ions are located at sites without inversion centres in $CaWO_4$ films [2], which is in agreement with the crystal

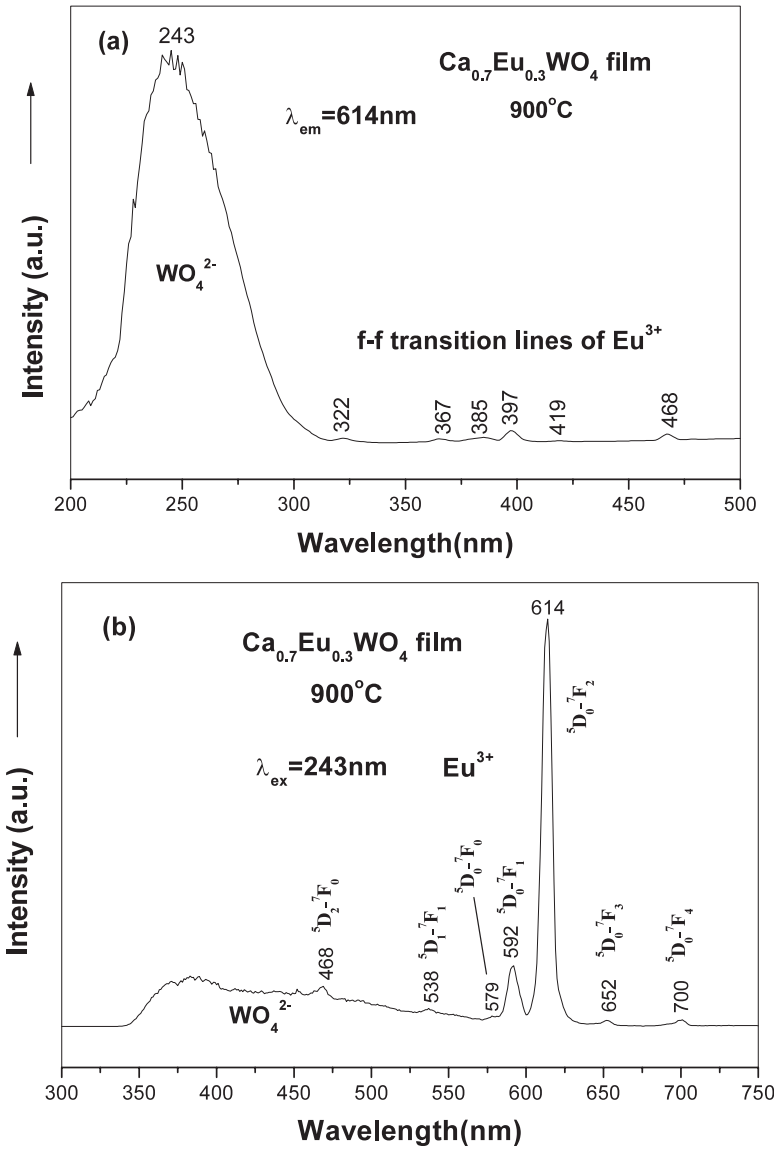

Figure 6. Excitation (a) and emission (b) spectra of $Ca_{0.7}Eu_{0.3}WO_4$ film annealed at 900 °C.

structure of $CaWO_4$. $CaWO_4$ crystallizes with the tetragonal scheelite structure and space group C_{4h}, in which the Ca^{2+} ion is coordinated by eight oxygen atoms and has a S_4 point symmetry (without an inversion centre) [27]. Obviously, the doped Eu^{3+} ion will substitute for the Ca^{2+} ion in the $CaWO_4$ host lattice in view of their close ionic radii. (The ionic radii of Eu^{3+} and Ca^{2+} are 0.107 and 0.112 nm for eight coordination, respectively [28].) As a result, the Eu^{3+} ion should hold a local site symmetry of S_4 in the $CaWO_4$ host lattice. Considering the different charges of Eu^{3+}(+3) and Ca^{2+}(+2), the actual site symmetry of Eu^{3+} might deviate from S_4 due to the charge compensating effects, i.e., $3Ca^{2+} \rightarrow 2Eu^{3+} + \square$ (defect). The presence of the very weak Eu^{3+} $^5D_0$–$^7F_0$ emission (579 nm), which is only allowed for C_s, C_n, and C_{nv} site symmetry [29], can confirm this viewpoint. The presence of emission lines

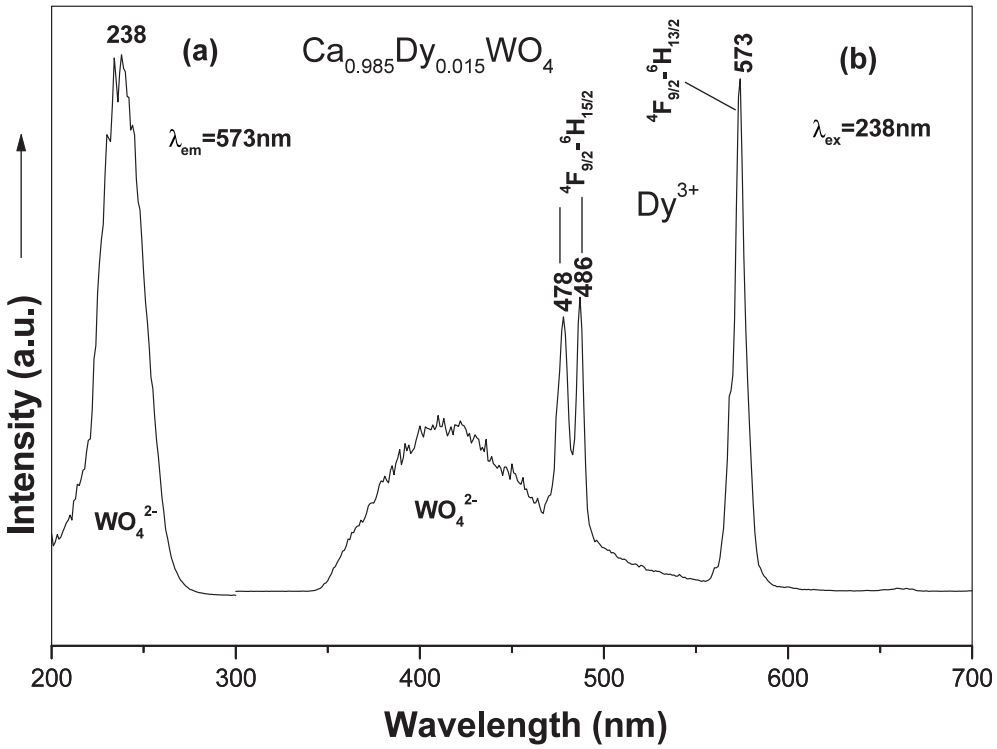

Figure 7. Excitation (a) and emission (b) spectra of $Ca_{0.985}Dy_{0.015}WO_4$ film annealed at 900 °C.

from higher excited states of Eu^{3+}($^5D_1$, $^5D_2$) is attributed to the low vibration energy of WO_4^{2-} groups (807 cm^{-1}, as indicated by figure 2). The multiphonon relaxation of WO_4^{2-} is not able to bridge the gaps between the higher energy levels ($^5D_1$, $^5D_2$) and the $^5D_0$ level of Eu^{3+} completely, resulting in the weak emissions from these levels. In silicates and borates where $\nu_{max} = 1000$–$1200\ cm^{-1}$, such emissions cannot be detected [2].

The same situation holds for the other $CaWO_4$ films doped with rare-earth ions Dy^{3+} and Sm^{3+}, Er^{3+}, as shown in figures 7 and 8, respectively. In the excitation spectra, the WO_4^{2-} excitation band at 238 nm for $Ca_{0.985}Dy_{0.015}WO_4$ film (figure 7(a)), at 235 nm for $Ca_{0.985}Sm_{0.015}WO_4$ film (figure 8(a), dashed–dotted curve), and at 241 nm for $Ca_{0.995}Er_{0.005}WO_4$ film (figure 8(a), solid curve) can be seen clearly, suggesting that the excitations in these films are also mainly via the WO_4^{2-} groups, i.e., an energy transfer from the WO_4^{2-} groups to Dy^{3+}, Sm^{3+}, Er^{3+} ions also occurs in $CaWO_4$ films. Upon excitation into the WO_4^{2-} absorption bands at maximum values, the emission spectra obtained also contain both the emission from the WO_4^{2-} and the characteristic transition lines of the rare-earth ions, i.e., the lines at 478, 486 nm ($^4F_{9/2}$–$^6H_{15/2}$), and 573 nm ($^4F_{9/2}$–$^6H_{13/2}$, dominant) for Dy^{3+} (figure 7(b)); at 563 nm ($^4G_{5/2}$–$^6H_{5/2}$), 596, 605 nm ($^4G_{5/2}$–$^6H_{7/2}$, dominant), and 646 nm ($^4G_{5/2}$–$^6H_{5/2}$) for Sm^{3+}; and at 520, 530 nm ($^2H_{11/2}$–$^4I_{15/2}$), and 542, 551 nm ($^4S_{3/2}$–$^4I_{15/2}$, dominant) for Er^{3+} (figure 8(b)). Since the emissions of Sm^{3+} and Er^{3+} are very weak compared with the emission band of WO_4^{2-}, it can be assumed that the efficiencies of energy transfers from WO_4^{2-} to Sm^{3+} and Er^{3+} are not as high as those of the energy transfers to Eu^{3+} and Dy^{3+} in $CaWO_4$ films.

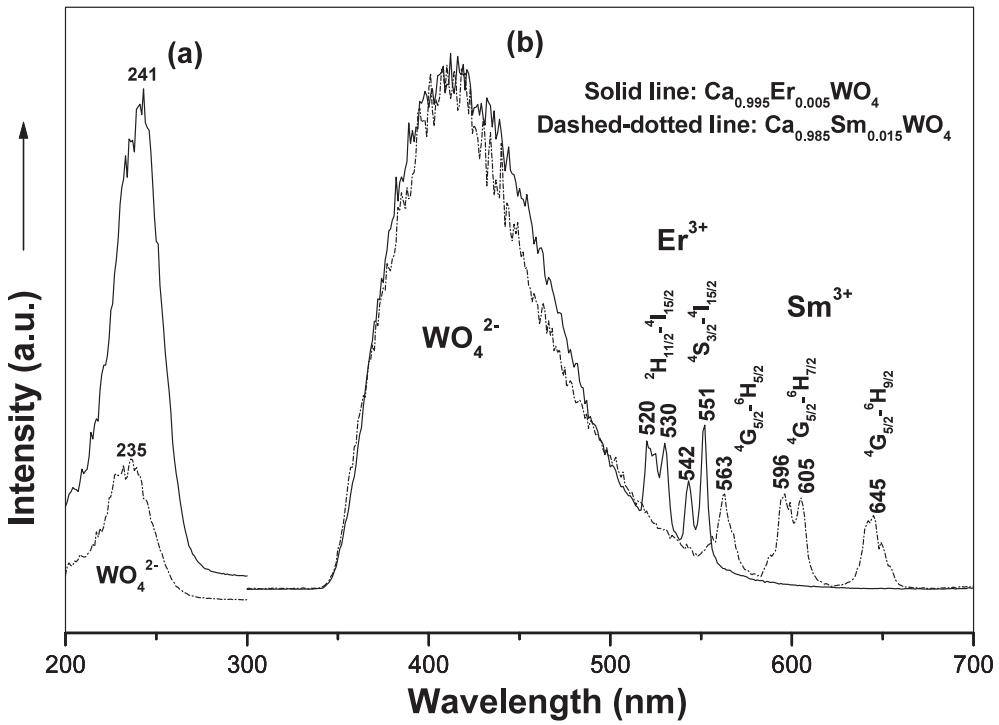

Figure 8. Excitation (a) and emission (b) spectra of $Ca_{0.985}Sm_{0.015}WO_4$ and $Ca_{0.995}Er_{0.005}WO_4$ films annealed at 900 °C.

Table 1. The effects of the annealing temperatures on the lifetimes (τ) and PL emission intensities (I) of the rare-earth (RE) ions (RE = Eu^{3+}, Dy^{3+}, Sm^{3+}, Er^{3+}) in $CaWO_4$ films (the doping concentrations of Eu^{3+}, Dy^{3+}, Sm^{3+}, Er^{3+} are 30, 1.5, 1.5, 0.5 at.% of Ca^{2+}, respectively).

		T (°C)				
RE		500	600	700	800	900
Eu^{3+}	I (au)	11 746	14 450	16 187	17 030	17 659
	τ (ms)	0.54	0.67	0.75	0.77	0.80
Dy^{3+}	I (au)	35 510	130 917	149 553	186 908	233 926
	τ (ms)	0.26	0.52	0.52	0.56	0.64
Sm^{3+}	I (au)	27 278	60 566	95 375	110 656	147 876
	τ (ms)	0.57	0.92	0.93	0.94	0.96
Er^{3+}	I (au)	25 269	120 082	210 127	250 444	352 560
	τ (ms)	0.008	0.028	0.029	0.030	0.031

Temperature effects. The lifetimes and PL emission intensities of rare-earth ions (Eu^{3+}, Dy^{3+}, Sm^{3+}, Er^{3+}) have been studied as a function of annealing temperature in $CaWO_4$ films. The decay curves for the luminescence of the rare-earth ions in the $CaWO_4$ films annealed at 900 °C are shown in figure 9. In general, these curves can be fitted to a single-exponential function: $I = I_0 \exp(-t/\tau)$ (where τ is the 1/e lifetime of the rare-earth ion). The lifetimes (τ) of excited states for $Eu^{3+}(^5D_0)$, $Dy^{3+}(^4F_{13/2})$, $Sm^{3+}(^4G_{5/2})$, and $Er^{3+}(^4S_{3/2})$ can be determined from the fittings. Table 1 lists the changes of the lifetimes and emission intensities of the rare-earth ions (Eu^{3+}, Dy^{3+}, Sm^{3+}, Er^{3+}) as a function of annealing temperature in $CaWO_4$

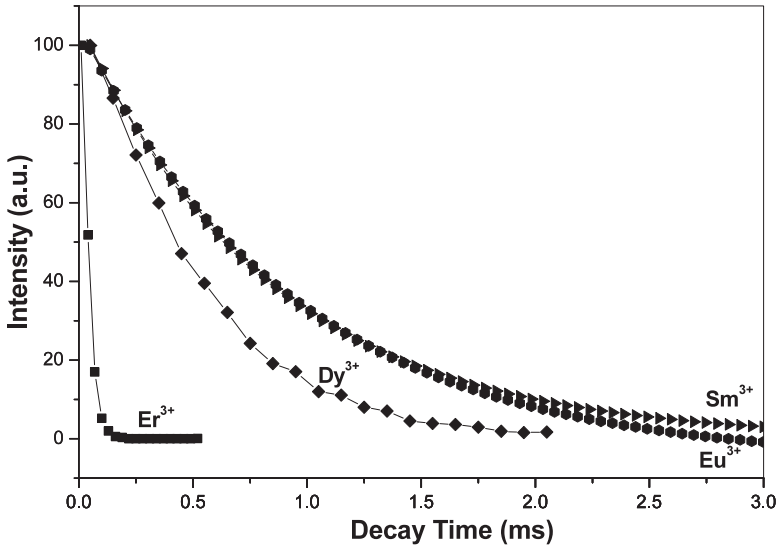

Figure 9. The decay curves of $Eu^{3+}(^5D_0–^7F_2$ at 614 nm), $Dy^{3+}(^4F_{9/2}–^6H_{13/2}$ at 572 nm), $Sm^{3+}(^4G_{5/2}–^6H_{7/2}$ at 605 nm), and $Er^{3+}(^4S_{3/2}–^4I_{15/2}$ at 551 nm) luminescence in crystalline $CaWO_4$ films annealed at 900 °C.

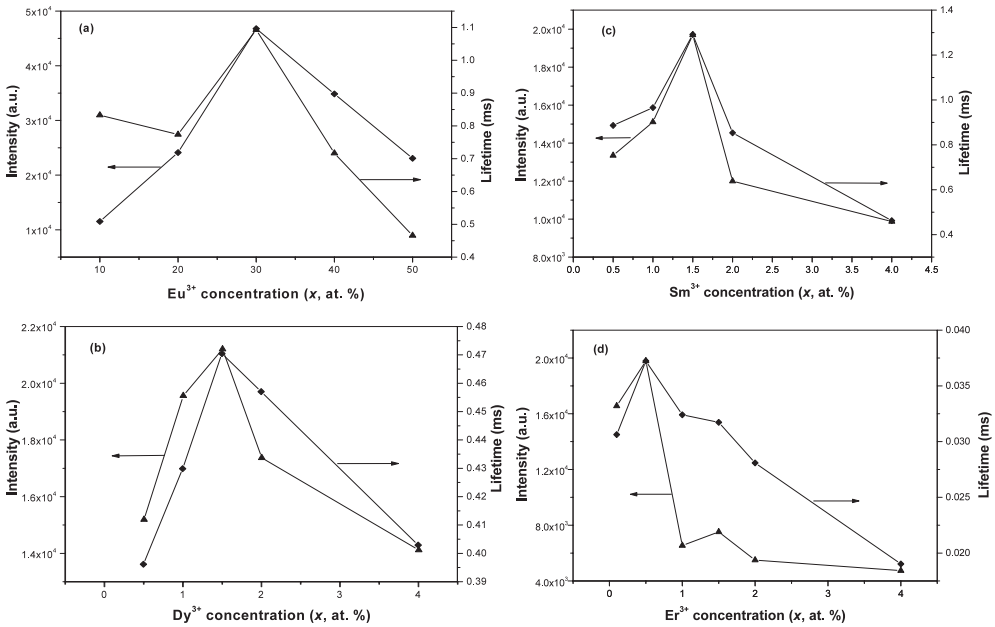

Figure 10. The PL emission intensity and lifetimes of rare earths (RE) as a function of their concentrations (x) in crystalline $Ca_{1-x}RE_xWO_4$ (RE = Eu^{3+}, Dy^{3+}, Sm^{3+}, Er^{3+}) films annealed at 900 °C.

films. From table 1 it can be seen that both the lifetimes and PL emission intensities for all four rare-earth ions increase with increase of the annealing temperature from 500 to 900 °C, as observed previously [20–22]. This is because with the increase of the annealing temperature,

the content of impurities, such as –OH, NO_3^-, and CH_2, in the film decreases and the degree of film crystallinity increases (as indicated by the XRD results in figure 1). The quenching of the luminescence of the rare-earth ions by the vibrations of these impurities decreases, resulting in the increase of the lifetimes and PL emission intensities.

Concentration effects. By varying the content of the rare-earth ions (Eu^{3+}, Dy^{3+}, Sm^{3+}, Er^{3+}) in $CaWO_4$ films, we determined the compositions with the highest PL emission intensities. Figures 10(a)–(d) show the dependence of the PL emission intensities and lifetimes of the rare-earth ion on its doping concentration (x) in $Ca_{1-x}RE_xWO_4$ (RE = Eu^{3+}, Dy^{3+}, Sm^{3+}, Er^{3+}) films, respectively. It can be found from figure 10 that the PL emission intensity of Eu^{3+}, Dy^{3+}, Sm^{3+}, Er^{3+} increases with increase of the concentration (x) at first, reaching a maximum value at $x = 0.3, 0.015, 0.015$, and 0.005 for Eu^{3+}, Dy^{3+}, Sm^{3+}, and Er^{3+} respectively, and then decreases with increasing content (x) due to the concentration quenching. Thus the optimum concentrations for Eu^{3+}, Dy^{3+}, Sm^{3+}, and Er^{3+} are 30, 1.5, 1.5, 0.5 at.% of Ca^{2+} in $CaWO_4$ films, respectively. The optimum concentrations for the four rare-earth ions agree well with those derived from the changes of their lifetimes as a function of the doping concentration (x) in $CaWO_4$ films, as shown in figures 10(a)–(d), respectively.

4. Conclusions

$CaWO_4$ phosphor films doped with rare-earth ions (Eu^{3+}, Dy^{3+}, Sm^{3+}, Er^{3+}) were successfully prepared by the Pechini sol–gel process using cheap and nontoxic inorganic compounds as the main precursors. The rare-earth ions Eu^{3+}, Dy^{3+}, Sm^{3+}, and Er^{3+} show their characteristic red ($^5D_0$–$^7F_2$), yellow ($^4F_{9/2}$–$^6H_{13/2}$), orange ($^4G_{5/2}$–$^6H_{7/2}$), and green ($^4S_{3/2}$–$^4I_{15/2}$) emissions in crystalline $CaWO_4$ phosphor films due to energy transfer from the WO_4^{2-} to them. The energy transfers from WO_4^{2-} to Eu^{3+} and Dy^{3+} are more efficient than those to Sm^{3+} and Er^{3+}. Both the lifetimes and PL intensities of the doped rare-earth ions increased with increase of the annealing temperature from 500 to 900 °C, and the optimum concentrations for Eu^{3+}, Dy^{3+}, Sm^{3+}, Er^{3+} were determined as 30, 1.5, 1.5, 0.5 at.% of Ca^{2+} in $CaWO_4$ films, respectively.

Acknowledgments

This project was financially supported by the foundation of 'Bairen Jihua' of the Chinese Academy of Sciences, the Outstanding Youth Fund of Jilin Province (20010103), the National Natural Science Foundation of China for Distinguished Young Scholars (50225205), and the Nanometre Centre of Changchun Institute of Applied Chemistry, Chinese Academy of Sciences.

References

[1] Saito N, Sonoyama N and Sakata T 1996 *Bull. Chem. Soc. Japan* **69** 2191
[2] Blasse G and Grabmaier B C 1994 *Luminescent Materials* (Berlin: Springer)
[3] Treadaway M J and Powell R C 1974 *J. Chem. Phys.* **61** 4003
[4] Grasser R and Scharmann A 1976 *J. Lumin.* **12/13** 473
[5] Johnson L F, Boyd G D, Nassau K and Soden R R 1962 *Phys. Rev.* **126** 1406
[6] Grasser R, Pitt E, Scharmann A and Zimmerer G 1975 *Phys. Status Solidi* b **69** 359
[7] Cho W S, Yashima M, Kakihana M, Kudo A, Sakata T and Yoshimura M 1995 *Appl. Phys. Lett.* **66** 1027
[8] Choe J Y, Ravichandran D, Blomquist S M, Morton D C, Kirchner K W, Ervin M H and Lee U 2001 *Appl. Phys. Lett.* **78** 3800
[9] Rabinovich E M, Shmulovich J, Fratello V J and Kopyov N J 1987 *Am. Ceram. Soc. Bull.* **6** 1505
[10] Lou Z D and Cocivera M 2002 *Mater. Res. Bull.* **37** 1573
[11] Kashiwakura Y and Kanehisa O 1989 *Japanese Patent Specification* 1-263188

[12] Carcia P F, Reilly M and Torardi C C 1997 *J. Mater. Res.* **12** 1385
[13] Cho Woo-seok, Yashima M and Kakihana M 1995 *J. Am. Ceram. Soc.* **78** 3110
[14] Min K W, Mho S I and Yeo I H 1999 *J. Electrochem. Soc.* **146** 3128
[15] Sakka S 1996 *Struct. Bonding* **85** 1
[16] Ravichandran D, Roy R, Chakhovskoi A G, Hunt C E, White W B and Erdei S 1997 *J. Lumin.* **71** 291
[17] Rao R P 1996 *Solid State Commun.* **99** 439
[18] Lin J, Saenger D U, Mennig M and Baerner K 2000 *Thin Solid Films* **360** 39
[19] Pechini M P 1967 *US Patent Specification* 3 330 697
[20] Yu M, Lin J, Wang Z, Wang S, Zhang H J, Fu J and Han Y C 2002 *Chem. Mater.* **14** 2224
[21] Yu M, Lin J, Zhou Y H, Wang S B and Zhang H J 2002 *J. Mater. Chem.* **12** 86
[22] Yu M, Lin J, Fu J, Zhang H J and Han Y C 2003 *J. Mater. Chem.* **13** 1413
[23] Burcham L J and Wachs I E 1998 *Spectrochim. Acta* A **54** 1355
[24] Grasser R, Scharmann A and Strack K R 1982 *J. Lumin.* **27** 263
[25] Grasser R and Scharmann A 1992 *Phys. Status Solidi* a **130** K99
[26] Blasse G 1980 *Structure and Bonding* vol 42 (Berlin: Springer)
[27] Page A G, Godbole S V and Sastry M D 1989 *J. Phys. Chem. Solids* **50** 571
[28] Shannon R D 1976 *Acta Crystallogr.* A **32** 751
[29] Blasse G and Bril A 1966 *Philips Res. Rep.* **2** 368